

Microrheology of semiflexible filament solutions based on relaxation simulations

L. K. R. Duarte,^{1,2} A. V. N. C. Teixeira,¹ and L. G. Rizzi¹

¹⁾*Departamento de Física, Universidade Federal de Viçosa (UFV), 36.570-900, Viçosa, MG, Brazil.*

²⁾*Instituto Federal de Educação, Ciência e Tecnologia de Minas Gerais, 35.588-000, Arcos, MG, Brazil.*

We present an efficient computational methodology to obtain the viscoelastic response of dilute solutions of semiflexible filaments. By considering an approach based on the fluctuation-dissipation theorem, we were able to evaluate the dynamical properties of probe particles immersed in solutions of semiflexible filaments from relaxation simulations with a relatively low computational cost and higher precision in comparison to those based on stochastic dynamics. We used a microrheological approach to obtain the complex shear modulus and the complex viscosity of the solution through its compliance which was obtained directly from the dynamical properties of a probe particle attached to an effective medium described by a mesoscopic model, *i.e.*, an effective filament model (EFM). The relaxation simulations were applied to assess the effects of the bending energy on the viscoelasticity of semiflexible filament solutions and our methodology was validated by comparing the numerical results to experimental data on DNA and collagen solutions.

1. INTRODUCTION

Despite of its importance to the well-functioning of almost all biological specimens¹, the assessment of the viscoelastic response of complex solutions of semiflexible filaments², *e.g.*, collagen, actin, rodlike viruses, amyloid fibrils, microtubules, and DNA, is still a difficult task to our current theoretical and computational approaches³. Contrary to solutions of cross-linked filaments, where a shear protocol can be used to extract the mechanical properties of the networks^{4–7}, the study of the viscoelastic response of solutions of diluted unentangled filaments relies mainly on indirectly monitoring the stochastic, *i.e.*, the fluctuating, dynamics of structures in the system^{8,9}. Alternatively, one could consider relaxation approaches which are based on the fluctuation-dissipation theorem (FDT), just as done experimentally in the microrheological characterization of complex solutions^{10–12}. However, even though computational simulations based on the FDT have been used to obtain the dynamics of systems with ideal networks^{13–15}, such relaxation simulations have not been applied to obtain the viscoelastic properties of solutions; that is the focus of the present study.

Previous computational efforts indicate that the characterization of the viscoelastic response of dilute solutions by first-principles, *i.e.*, molecular-based, approaches can be very challenging¹⁶. Although simulations considering atomistic models might be able to account for detailed molecular interactions including, *e.g.*, polymer-solvent interactions and also hydrodynamic effects between different polymeric chains, they can be hardly used to retrieve the relaxation behaviour of the structures in the system that is required to describe the viscoelastic response of the solutions at the experimentally relevant (*i.e.*, mesoscopic) time and length scales, *e.g.*, milliseconds and micrometers. Even so, such detailed simula-

tions might provide the basis for systematic coarsening procedures¹⁶, but here we restrict ourselves to a less ambitious yet complementary modelling approach that is based on the microrheological characterization of the solutions, where the relaxation behaviour of the system is extracted from the dynamics of probe particles immersed in the medium¹⁷.

For simplicity, we consider that the effects of the coupling between micron-sized probe particles and the dilute solution of filaments can be described by the dynamics of tagged beads in the middle of an effective mesoscopic model. Our idea is to assume the simplest constitutive approach which lead to relaxation behaviours that are similar to the ones that are observed for polymeric solutions. Thus, we focus our attention to demonstrate how the relaxation simulations can be used to efficiently extract the non-markovian dynamics of the probe particles that ultimately allows one to determine the frequency-dependent shear moduli and complex viscosity that are characteristic of viscoelastic solutions of semiflexible filaments.

The reminder of the paper is as follows. First, in Sec. 2, we review some of the relevant theoretical and computational aspects related to the rheology and microrheology of solutions of unentangled filaments. In Sec. 3 we describe a simple mesoscopic constitutive model that is used to mimic the effective response of the solutions and present the numerical methods commonly adopted to perform stochastic simulations. In Sec. 4 we discuss the approach based on relaxation simulations, which allow us to extract the viscoelastic properties of solutions from the dynamics of the probe particles described by the effective mesoscopic model. Also, we validate our methodology by including a comparison between the results obtained from the relaxation simulations and the stochastic simulations, as well as a comparison between the numerically obtained

results and the experimental data obtained for solutions of polyelectrolytes. The results for semiflexible filaments are presented in Sec. 5, where we investigate the effects of bending energies on the viscoelasticity of dilute solutions and we also include comparisons between the numerical results and the experimental data obtained for DNA and collagen macromolecules.

2. VISCOELASTICITY OF UNENTANGLED SOLUTIONS

2.1. Viscoelastic response functions

Experimentally, one can characterize the mechanical properties of viscoelastic fluids by considering, *e.g.*, steady-state shearing experiments¹⁸, where the time-dependent stress $\sigma(t)$ of the viscoelastic material is related to its relaxation modulus $G(\tau)$ as^{19,20}

$$\sigma(t) = \int_{-\infty}^t dt' G(t-t') \dot{\gamma}(t') , \quad (1)$$

with $\dot{\gamma}$ being the shear rate. Also, one can consider small-amplitude oscillatory shearing experiments¹⁸ with $\gamma(t)$ being an oscillatory function so that the viscoelastic response of the fluid is given by the complex shear modulus, $G^*(\omega) = G'(\omega) + iG''(\omega)$, where $G'(\omega)$ and $G''(\omega)$ correspond to the storage and the loss modulus, respectively. At the linear viscoelastic (LVE) response regime, both experimental techniques should provide the same information, as the complex modulus is directly related to $G(\tau)$ via a Fourier transform^{18,21}, that is,

$$G^*(\omega) = i\omega \int_0^\infty d\tau' G(\tau') e^{-i\omega\tau'} . \quad (2)$$

For viscoelastic solutions, it is also convenient to obtain the complex viscosity¹⁸, $\eta^*(\omega) = \eta'(\omega) - i\eta''(\omega)$, which is related to the complex modulus as $G^*(\omega) = i\omega\eta^*(\omega)$, so that $\eta'(\omega) = G''(\omega)/\omega$ and $\eta''(\omega) = G'(\omega)/\omega$. At low frequencies, the loss modulus of viscoelastic solutions is expected to be proportional to the frequency, *i.e.*, $G''(\omega) \propto \omega$, so the viscosity $\eta'(\omega)$ should be independent of the frequency and is related to the relaxation modulus as²¹

$$\eta_0 = \lim_{\omega \rightarrow 0} \eta'(\omega) = \int_0^\infty d\tau' G(\tau') , \quad (3)$$

which is, according to the Cox-Merz rule, equivalent to the steady-state viscosity $\eta(\dot{\gamma}) = \sigma(\dot{\gamma})/\dot{\gamma}$ that is obtained for low shear rates at the LVE regime²².

2.2. Microrheology

Alternatively, the viscoelasticity of complex solutions can be obtained through microrheological techniques^{17,23}, which are based on relationships between the

viscoelastic response of the material and the dynamics of probe particles immersed in it (see, *e.g.*, Ref.²⁴). In particular, one can explore passive experimental approaches (*e.g.*, particle tracking videomicroscopy or dynamic light scattering; see Ref.¹⁷ for a review) to extract the mean-squared displacement (MSD) $\langle \Delta r^2(\tau) \rangle_a$ of probe particles with radius a and relate it to the compliance $J(\tau)$ of the solution through a generalized Stokes-Einstein relationship^{23,25,26}, that is,

$$J(\tau) = \frac{3\pi a}{dk_B T} \langle \Delta r^2(\tau) \rangle_a , \quad (4)$$

where d is the euclidean dimension of the random walk, k_B is the Boltzmann's constant, and T is the absolute temperature of the medium. A simple way to understand this relationship is by considering the diffusion of the probe particles at later times, *i.e.*, at times τ that are longer than the longest relaxation time τ_f of the solution. In that case one should observe a normal diffusive behaviour where the MSD is given by $\langle \Delta r^2(\tau) \rangle_a = 2dD_a\tau$ with

$$D_a = \frac{k_B T}{6\pi a \eta_0} , \quad (5)$$

so that the right hand side of Eq. (4) yields τ/η_0 , which is the compliance $J(\tau)$ that one would measure from creep-compliance experiments, *i.e.*, which is independent of the radius a of the probe particles. Importantly, the above expression is valid only for relatively large and isolated particles which effectively probe the viscosity η_0 of the solution²³ (usually, micron-sized beads are chosen to probe the LVE response of polymeric solutions¹).

At the LVE regime, microrheology and rheology are expected to give the same information about the viscoelastic behaviour of the solution. Also, one should note that the relaxation modulus is linked to the compliance $J(\tau)$ of the solution through a convolution¹⁹,

$$\int_0^\tau G(\tau - \tau') J(\tau') d\tau' = \tau , \quad (6)$$

and one can evaluate the complex shear modulus directly from the Fourier transform of the compliance $\hat{J}(\omega)$ as

$$G^*(\omega) = \frac{1}{i\omega \hat{J}(\omega)} . \quad (7)$$

2.3. Stochastic dynamics and relaxation of polymers

Theoretically, the viscoelastic response of diluted unentangled filament solutions can be evaluated through estimates of the intrinsic relaxation modulus²⁷ $[G(\tau)]$. Based on polymer physics, one may resort to a heuristic argument that the relaxation times will depend on the relaxation of partial segments of the filaments so that an approximated expression for the relaxation modulus can

be written as^{20,21}

$$G(\tau) \propto n_f k_B T \left(\frac{\tau}{\tau_f} \right)^{-\alpha} e^{-(\tau/\tau_f)} , \quad (8)$$

where n_f is the number density of filaments, τ_f is the longest relaxation time of the filaments in solution, and α is an exponent that characterizes the effective flexibility of the filaments^{20,21}. By inserting $G(\tau)$ into expression (2) one finds that the frequency-dependent shear moduli present a power-law behaviour with the same exponent, that is, $G'(\omega) \propto G''(\omega) \propto \omega^\alpha$, at intermediate frequencies (*i.e.*, $\omega > \omega_f$ with $\omega_f = 1/\tau_f$).

Interestingly, by assuming the same heuristic principle, numerical results obtained from simulations using single chains^{28,29} have also suggested that the relaxation behaviour of dilute solutions at intermediate times, *i.e.*, $\tau < \tau_f$, should be somewhat related to the stochastic dynamics of the monomers in the middle of the polymeric chains. It seems that the intrinsic relaxation modulus should show a power-law behaviour which display the same characteristic exponent of the subdiffusive behaviour observed for the MSD of the monomeric units in the polymeric chain, that is, $\langle \Delta r^2(\tau) \rangle_m \propto \tau^\alpha$, with $\alpha < 1$. For semiflexible chains, in particular, recent molecular dynamics simulations³⁰ indicate that the MSD of monomeric units display an exponent $\alpha = 3/4$, which agreed with several theoretical approaches^{20,31} and experimental evidence^{3,32-34} in the literature. Numerical simulations presented in Ref.³⁰ confirmed the results obtained in Refs.^{29,35,36} that both bond autocorrelation and end-to-end vector correlation functions (which are extracted from an isolated chain and can be related to the intrinsic relaxation modulus), display a power-law behaviour that lead to a similar exponent.

As discussed in Refs.^{37,38}, one can actually use a generalized theoretical Langevin approach to recover the same relaxation behaviour given by Eq. (8) with $\alpha = 1/2$ (*i.e.*, for Rouse chains) in the overdamped regime by considering the non-markovian dynamics of a tagged particle in the middle of a flexible chain. In addition, Reference³⁹ shows that it is possible to consider a similar generalized Langevin approach to link the shear moduli of a viscoelastic material to the dynamics of a probe particle through a microrheological approach based on Eq. (4). Hence, in order to demonstrate the usefulness of the relaxation simulations introduced here without having to resort to atomistic simulations, we consider a mesoscopic constitutive model that effectively describes the non-markovian dynamics of a probe particle immersed in a mesoscopic region of a dilute solution of filaments, just as shown in Fig. 1(a).

3. NUMERICAL METHODS

Before getting into how one can obtain the viscoelastic response functions from the relaxation simulations, we introduce in this Section the aforementioned mesoscopic

model used to describe the coupling between the probe particle and the dilute solution of filaments, as well as the numerical procedures used to obtain its dynamical properties from stochastic simulations which are explored latter to validate our relaxation-based approach.

3.1. Effective filament model (EFM)

As illustrated in Fig. 1(a), we represent a probe particle in a mesoscopic region of the solution of filaments by an effective filamentous structure (*i.e.*, the EFM) which is modelled by a simple bead-spring model with N beads in an implicit solvent that has the same properties of the original solution, *i.e.*, its viscosity η_s and temperature T . The beads in such EFM are coupled to their nearest neighbours by an interaction potential that can include

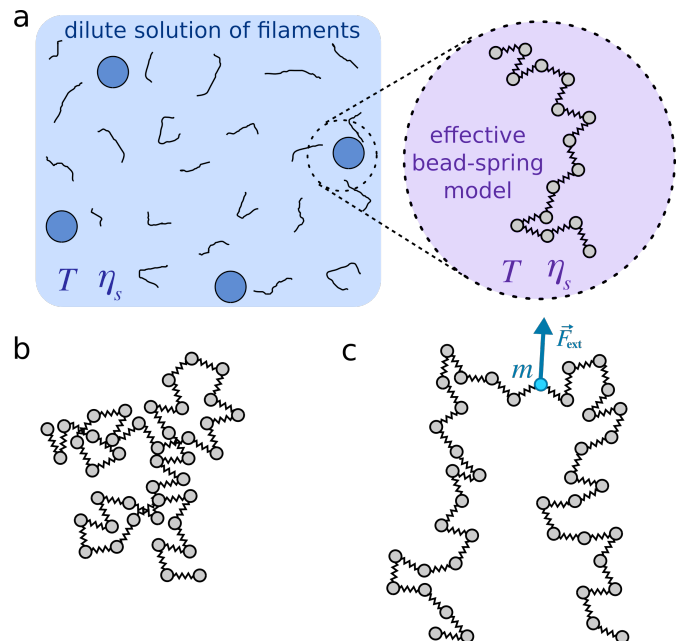


FIG. 1. (a) The dynamics of a probe particle (blue circle) immersed in a mesoscopic region of the solution of diluted filaments (left panel) is effectively described by the dynamics of a bead (grey circles) in a bead-spring model (right panel). The effective filament model (EFM) at the right panel is used as a constitutive model to describe the relaxation of solutions of both flexible and semiflexible filaments. The non-markovian dynamics of beads in the EFM depends on their interactions, which are determined by effective elastic (κ) and bending (κ_b) constants defined in Eqs. (9) and (10), respectively. The link between the EFM (right panel) and the viscoelastic properties of the corresponding solution (left panel) is made through the diffusion coefficients D_a , Eq. (5), and D_f , Eq. (22), which are defined in terms of the radius a of the probe particle. (b) Typical configuration of the EFM in the overdamped Langevin approach, where the dynamics of its beads is stochastic. (c) Configuration in the relaxation approach, where an external force \vec{F}_{ext} is used to pull the m -th bead placed in the middle of the EFM.

contributions from both harmonic (U_h) and bending (U_b) energies.

The harmonic interaction potential of the whole effective filament is written as

$$U_h = \frac{\kappa}{2} \sum_{j=1}^{N-1} (\vec{r}_{j+1} - \vec{r}_j)^2, \quad (9)$$

where \vec{r}_j is the position vector of the j -th bead and κ is the effective elastic constant. One can relate the pre-factor in Eq. (9) to the pre-factor of the Gaussian chain model²⁷, so that $\kappa = 3k_B T/b^2$, where b is a parameter that sets the length scale (*e.g.*, nm) and the strength of the harmonic interaction.

For the bending interaction potential we assume its discretized approximation (see, *e.g.*, Ref.⁴⁰), which is evaluated as the sum of local curvatures along the EFM and is given by

$$U_b = \frac{\kappa_b}{2} \sum_{j=2}^{N-1} (\vec{r}_{j-1} - 2\vec{r}_j + \vec{r}_{j+1})^2, \quad (10)$$

where $\kappa_b = E/b^4$ is the bending constant, with E being a parameter that sets the bending stiffness. Both constants κ and κ_b are given in units of force per length, *e.g.*, pN/nm. The value of κ_b can be approximately related to the persistent length of the filament L_p , since it should be proportional to $A \equiv E'/b$, with $E' = E/k_B T$ (*e.g.*, if E is given in pN.nm³ and b in nm, E' is given in nm², and L_p and A in nm).

3.2. Stochastic simulations

First, in order to validate the relaxation simulations, we compare it to stochastic, *i.e.*, Brownian dynamics, simulations, which consist in solving numerically the overdamped Langevin equation. For the i -th bead in the EFM, such equation is written as

$$\frac{\partial \vec{r}_i}{\partial t} = \frac{1}{\zeta} \left(\vec{F}_i + \vec{f}_a \right), \quad (11)$$

where \vec{f}_a is a random force due to interaction of the bead with the implicit effective solvent, ζ is a time-independent friction coefficient, and \vec{F}_i is the total force exerted on the i -th bead which is determined from the interaction potentials defined by Eqs. (9) and (10), *i.e.*, $\vec{F}_i = -\nabla_i(U_h + U_b)$, with $\nabla_i = \partial_{x_i} \hat{x} + \partial_{y_i} \hat{y} + \partial_{z_i} \hat{z}$.

In practice, one have $3N$ coupled differential equations defined as in Eq. (11), which are discretized and solved numerically by considering the Euler integration scheme, so that the position vector of the i -th bead at a time $t + \Delta t$ is given by

$$\vec{r}_i(t + \Delta t) = \vec{r}_i(t) + \frac{\Delta t}{\zeta} \left(\vec{F}_i + \vec{f}_a \right), \quad (12)$$

where the k -th component of the random force is evaluated as⁴¹

$$f_{a,k} = \sqrt{\frac{2\zeta k_B T}{\Delta t}} N_k(0, 1), \quad (13)$$

with $N_k(0, 1)$ (for $k = x, y$, or z) being independent random variables obtained from a gaussian distribution with zero mean and variance equal to one. We assume that the value of the effective friction coefficient ζ depends on the radius a of the probe particle and is determined by the Stokes-Einstein relation, that is,

$$\zeta = \frac{k_B T}{D_0} = 6\pi a \eta_s, \quad (14)$$

where $D_0 = k_B T/6\pi a \eta_s$ defines the diffusion coefficient of a non-connected bead, *i.e.*, a probe particle with radius a freely diffusing in a solvent with viscosity η_s .

Hence, we impose that the dynamics of probe particles in the solution of filaments given by $\langle \Delta r^2(\tau) \rangle_a$ can be effectively characterized by the fluctuations in the position of the beads of the EFM, which are quantified by their mean-squared displacement,

$$\langle \Delta r^2(\tau) \rangle = \langle [\vec{r}(\tau + t_0) - \vec{r}(t_0)]^2 \rangle, \quad (15)$$

where $\langle \dots \rangle$ denote averages over both N_T beads and M realizations of the numerical experiment. The initial configuration in each numerical simulation corresponds to a fully stretched chain with the beads separated by a distance b , and the averages are evaluated only after a thermalization period of time t_0 .

The time-dependent diffusion coefficient $D(\tau)$ of the beads in the EFM can be retrieved from the time derivative of the MSD of the bead's position, that is

$$D(\tau) = \frac{1}{2d} \frac{\partial \langle \Delta r^2(\tau) \rangle}{\partial \tau}. \quad (16)$$

For all simulations we consider that the euclidean dimension is $d = 3$. It is worth mentioning that, in order to avoid boundary effects on $\langle \Delta r^2(\tau) \rangle$ and $D(\tau)$, we consider that the average value is evaluated over the $N_T = N - 2N_E$ beads which are centrally localized in the chain, *i.e.*, excluding N_E beads on each side of the EFM.

3.3. Flexible EFM

In order to illustrate the dynamics of the EFM and validate our relaxation approach we present in Fig. 2 a comparison between the two methods for the MSD and the time-dependent diffusion coefficient obtained for a flexible EFM, *i.e.*, without bending energy (the relaxation approach will be described in the next section). Without bending energies, the dynamics of the beads in the EFM can be quantitatively described by the Rouse model^{20,27} and, as expected, the MSD displays two normal diffusion

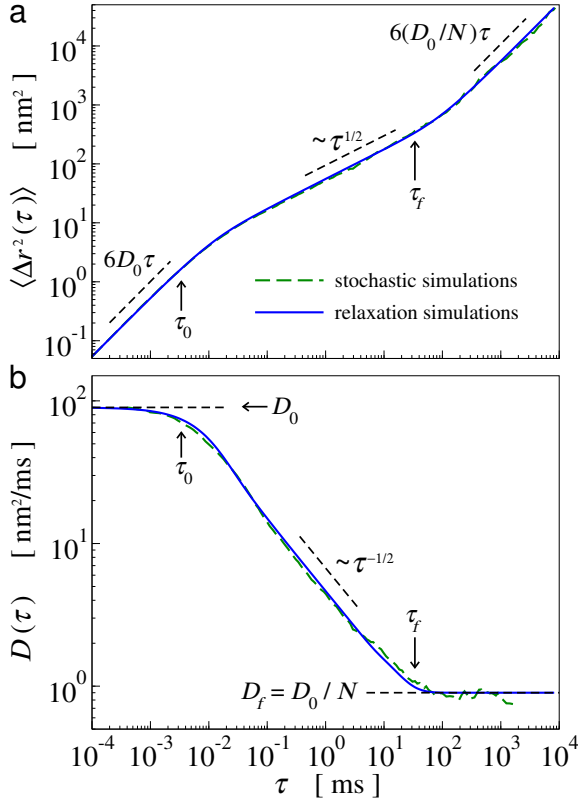


FIG. 2. (a) Mean-squared displacement $\langle \Delta r^2(\tau) \rangle$, and (b) time-dependent diffusion coefficient $D(\tau)$, as function of time τ , for a flexible EFM (*i.e.*, no bending energy, $\kappa_b = 0$ pN/nm). Long-dashed green lines correspond to stochastic simulations, while straight blue lines correspond to relaxation simulations. Short-dashed black lines indicate the two normal diffusive behaviours where $\langle \Delta r^2(\tau) \rangle \propto \tau$ and $D(\tau)$ is constant, and the intermediate subdiffusive behaviour with $\langle \Delta r^2(\tau) \rangle \propto \tau^{1/2}$ and $D(\tau) \propto \tau^{-1/2}$, as expected from Rouse dynamics²⁷ (see text for details). For both numerical approaches the results were obtained with the arbitrary parameters $N = 100$, $D_0 = 90$ nm²/ms, $\kappa = 1.38$ pN/nm ($b = 3$ nm), and $T = 300$ ($k_B T = 4.142$ pN.nm), so that $\tau_0 = k_B T / (\pi^2 \kappa D_0) \approx 0.0034$ ms, and $\tau_f = \tau_0 N^2 \approx 34$ ms. For the stochastic simulations, the results correspond to average values obtained from $M = 100$ realizations with $N_E = 7$ after a thermalization of $t_0 = 5 \times 10^2$ ms (*i.e.*, 5×10^6 steps with $\Delta t = 10^{-4}$ ms). For the relaxation simulations a constant external force $F_0 = 1$ pN and the same Δt were considered but no thermalization was required.

regimes: one for times shorter than $\tau_0 = k_B T / (\pi^2 \kappa D_0)$, with $\langle \Delta r^2(\tau) \rangle = 6D_0\tau$, which corresponds to the free-like displacements of the beads; and the other for times longer than $\tau_f = \tau_0 N^2$, with $\langle \Delta r^2(\tau) \rangle = 6(D_0/N)\tau$, which corresponds to the diffusion of the centre of mass of the EFM. Also, the Rouse model predicts an intermediate regime with a characteristic subdiffusive anomalous behaviour²⁷, where $\langle \Delta r^2(\tau) \rangle = \sqrt{36k_B T D_0 / (\pi \kappa)} \tau^{1/2}$. As shown in Fig. 2(b), those regimes are better identified by the time-dependent diffusion coefficient $D(\tau)$, which shows a transient power-law regime, *i.e.*, $D(\tau) =$

$\sqrt{k_B T D_0 / (4\pi \kappa)} \tau^{-1/2}$, between two plateaus, one with $D(\tau) = D_0$ at times shorter than $\tau_0 \approx 0.0034$ ms, and the other with $D(\tau) = D_f = D_0/N$, at times longer than $\tau_f \approx 34$ ms.

4. RELAXATION APPROACH

In this Section we describe the theory and the numerical procedures involved in the relaxation simulations that are used to obtain the dynamical properties of the EFM, as well as how those properties can be used to provide numerical estimates for the shear moduli and the complex viscosity of the corresponding diluted filament solutions.

4.1. Relaxation simulations based on the FDT

In the relaxation approach, the MSD $\langle \Delta r^2(\tau) \rangle$ and the time-dependent diffusion coefficient $D(\tau)$ of the beads in the EFM are evaluated from a relation that comes from the fluctuation-dissipation theorem (FDT)^{21,27}.

Importantly, the use of the relaxation simulations based on FDT is restricted to the linear response regime, which means that the intensity of the external force is relatively weak but large enough so that one can neglect the random thermal forces \vec{f}_a . In this case one can solve the $3N$ coupled differential equations by using a Euler integration scheme similar to Eq. (12), but assuming that \vec{f}_a are close to zero, so that

$$\vec{r}_i(t + \Delta t) = \vec{r}_i(t) + \frac{\Delta t}{\zeta} \left(\vec{F}_i + \delta_{im} \vec{F}_{\text{ext}} \right), \quad (17)$$

where the Kronecker's delta δ_{im} indicates that the constant external force $\vec{F}_{\text{ext}} = F_0 \hat{z}$ is applied only to the m -th bead in the middle of the EFM, as illustrated in Fig. 1(c).

In practice, the FDT can be used to link the displacement $\Delta z(\tau)$ of the m -th bead driven by an external force to the fluctuations on its position at equilibrium as²¹

$$\Delta z(\tau) = [z_m(\tau) - z_m(0)] = \chi_{zz}(\tau) F_0, \quad (18)$$

where $\chi_{zz}(\tau)$ is a linear response function given by

$$\chi_{zz}(\tau) = \frac{1}{2k_B T} \langle \Delta z^2(\tau) \rangle. \quad (19)$$

Hence, one can estimate the MSD of the beads in d dimensions as

$$\langle \Delta r^2(\tau) \rangle = \frac{2dk_B T}{F_0} [z_m(\tau) - z_m(0)]. \quad (20)$$

Also, one can retrieve the time-dependent diffusion coefficient $D(\tau)$ by derivating Eq. (20) just as prescribed by Eq. (16), which yields

$$D(\tau) = \frac{k_B T}{F_0} v_{m,z}(\tau), \quad (21)$$

where $v_{m,z}(\tau)$ is the velocity of the m -th bead, which can be directly obtained from the numerical integration scheme.

As one can see in Fig. 2, the results obtained from the relaxation approach with Eqs. (20) and (21) display a good agreement to those obtained from the stochastic simulations. It is worth mentioning that, since one does not have to compute averages over M realizations and it does not require the thermalization step (*i.e.*, the initial configuration corresponds to a fully stretched chain placed along a direction that is perpendicular to z with a separation b between beads), the numerical approach based on relaxation dynamics is far more efficient than the one based on stochastic dynamics. For instance, the results obtained from relaxation simulations presented in Fig. 2 took less than a minute to be produced, while the simulations using the stochastic approach required several hours. Also, the numerical data obtained from relaxation simulations is not noisy as those obtained from the stochastic simulations. That is very convenient since, as we discuss in the following, one has to compute Fourier transforms of $\langle \Delta r^2(\tau) \rangle$ in order to extract the viscoelastic properties of the solutions.

It is worth noting that, since the FDT expressions are very general, the relaxation approach based on Eqs. (20) and (21) could be applied to models other than the EFM defined in Sec. 3.1, *e.g.*, molecular-based models with explicit solvent, just as it is done in experiments¹¹. Even so, just to illustrate the determination of the viscoelastic functions from those equations, we discuss in the next Section how one can explore the relationship between the EFM and the Rouse model to describe the experimental data.

4.2. Viscoelastic properties

As discussed in Sec. 2, the viscoelastic properties of the filament solution are characterized by the complex shear modulus $G^*(\omega) = G'(\omega) + iG''(\omega)$, which can be evaluated from the Fourier transform of the compliance of the solution $J(\tau)$ based on Eq. (7). The idea of using an approach based on microrheology is that one can obtain $J(\tau)$ directly from the dynamics of probe particles, *e.g.*, from the MSD of the beads in the EFM, through Eq. (4).

For the EFM, in particular, the first task is to obtain its effective parameters (*i.e.*, N , D_0 , κ , and κ_b) in order to describe the full behaviour of all the viscoelastic functions, *i.e.*, $J(\tau)$, $G'(\omega)$, $G''(\omega)$, $\eta'(\omega)$, by considering only a minimal experimentally available information, *e.g.*, T , η_s , η_0 , and τ_f . In order to illustrate how that can be done, we first consider dilute solutions of polyelectrolyte chains. In particular, in Fig. 3 we include a comparison between the results obtained from our relaxation simulations and the experimental data presented in Ref.¹¹ on a solution of polyacrylamide (PAM) chains.

As discussed in Sec. 3.3 and illustrated by the numerical results presented in Fig. 2, the dynamics of the beads

in the flexible EFM can be well described by the Rouse model, so that the limiting values for the time-dependent diffusion coefficient $D(\tau)$ are given by D_0 for $\tau \ll \tau_0$ (see Eq. (14)), and by

$$D_f = \frac{D_0}{N} = \frac{k_B T}{6\pi a \eta_s N} , \quad (22)$$

for $\tau \gg \tau_f$, where the longest relaxation time of the EFM is given by the Rouse relaxation time²⁷, that is,

$$\tau_f = \frac{k_B T}{\pi^2 \kappa D_0} N^2 . \quad (23)$$

Hence, by assuming that the diffusion coefficient D_f given by Eq. (22) should be equal to the diffusion coefficient D_a of a probe particle with radius a defined by Eq. (5), one can readily identify that the relative viscosity of the solution, η_r , is related to the effective number of beads N of the EFM as

$$\eta_r = \frac{\eta_0}{\eta_s} = N . \quad (24)$$

This expression is very useful since it allows one to estimate the effective number of beads N which the EFM needs in order to correctly describe the experimental data. For instance, the value $N = 10$ can be inferred from Fig. 3(c) by realizing that the frequency-dependent viscosity $\eta'(\omega)$ is given approximately by $\eta_\infty = \lim_{\omega \rightarrow \infty} \eta'(\omega) = \eta_0/N = \eta_s$ at high frequencies, and by $\eta_0 = \lim_{\omega \rightarrow 0} \eta'(\omega)$, at low frequencies. Alternatively, one can also obtain the value of N from Eq. (22) by measuring the diffusion coefficients D_0 and D_f from the MSD data (as in Fig. 2), even so, such procedure would be equivalent to the aforementioned approach based on $\eta'(\omega)$, this because the MSD and the compliance are related through Eq. (4) and, as shown in Fig. 3(a), one has that $J(\tau) = \tau/\eta_s$ for $\tau \ll \tau_0$ and $J(\tau) = \tau/\eta_0$ for $\tau \gg \tau_f$.

It is worth mentioning that, since η_r should depend on both the number density n_f and the molecular weight M_f of the filaments²⁰, Eq. (24) tells us that, at least for dilute solutions, the number of beads N of the EFM should also present a similar dependence on those quantities. Here we recall that the concentration of filaments w_f (given in % w/w) is related to the number density as $w_f = n_f M_f / (n_s M_s + n_f M_f)$, where n_s and M_s are the number density and molecular weight of the solvent molecules, respectively. Hence, by considering that the molecular weight of PAM chains is $M_{\text{PAM}} = 18 \times 10^6$ g/mol (see Ref.¹¹), the number density and the molecular weight of water molecules are, respectively, $n_{\text{water}} = 3.34 \times 10^{22}$ cm⁻³ and $M_{\text{water}} = 18$ g/mol, and that the concentration used in the experiments¹¹ was $w_{\text{PAM}} = 0.07\%$ w/w, one finds that the number density of PAM chains is $n_{\text{PAM}} \approx 2.33 \times 10^{13}$ cm⁻³. By assuming a relaxation modulus $G(\tau)$ similar to the one defined by Eq. (8) one can evaluate the low-frequency viscosity η_0 of dilute solutions through Eq. (3), which yields

$$\eta_0 \approx \frac{4}{3} n_f k_B T \tau_f . \quad (25)$$

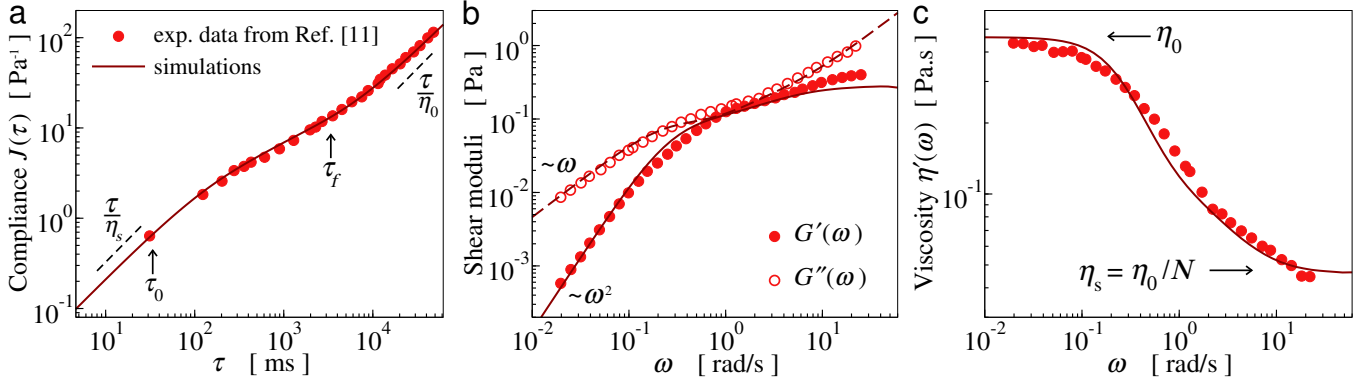


FIG. 3. Comparison between the experimental data (circles) on flexible polyelectrolyte chains extracted from Ref.¹¹ and the numerical results obtained from the relaxation simulations (continuous lines). (a) Compliance $J(\tau)$, (b) storage modulus $G'(\omega)$ (filled circles) and loss modulus $G''(\omega)$ (open circles), and (c) viscosity, $\eta'(\omega)$. Numerical estimates for the MSD of the EFM beads $\langle \Delta r^2(\tau) \rangle$ were obtained via Eq. (20) from relaxation simulations implemented with $F_0 = 1$ pN, $N = 10$, $D_0 = 1.69$ nm²/ms, $\kappa = 7.28 \times 10^{-3}$ pN/nm ($b \approx 41$ nm), and $\Delta t = 0.1$ ms (the specific values of D_0 and κ were determined respectively through Eqs. (22) and (26) by setting the radius of the probe particles equal to $a = 2.8$ μ m as in Ref.¹¹). The match between the compliance $J(\tau)$ obtained from our numerical simulations through Eq. (27) and the experimental data of Ref.¹¹ was done by considering $\eta_0 \approx 460$ mPa.s, $\eta_s \approx 46$ mPa.s, $T \approx 25^\circ\text{C}$ ($k_B T = 4.114$ pN.nm), and $\tau_f \approx 3.38$ s (*i.e.*, $\tau_f \approx 3.38 \times 10^3$ ms). Those values yield a number density equal to $n_f = 2.5 \times 10^{13}$ cm⁻³ that is close to the value n_{PAM} obtained from the nominal concentration of 0.07% w/w used in the experiments (see text for details). The complex shear modulus, $G^*(\omega)$, and the viscosity, $\eta'(\omega) = G''(\omega)/\omega$, were obtained from $J(\tau)$ via Eq. (7) using the numerical method described in Ref.⁴².

Although a similar expression can be obtained specifically for flexible filaments^{20,21} by considering $G(\tau)$ defined by Eq. (8) with $\alpha = 1/2$, it seems that approximated expressions, *i.e.*, with slightly different pre-factors, should be valid for complex fluids in general³⁹. Indeed, by assuming that $\eta_0 \approx 460$ mPa.s, $\tau_f \approx 3.38$ s, and that the experiments with PAM¹¹ were done at $T = 25^\circ\text{C}$ (*i.e.*, $k_B T = 4.114$ pN.nm), Eq. (25) yields $n_f \approx 2.5 \times 10^{13}$ cm⁻³, which is in good agreement with the value of n_{PAM} estimated from the molecular weights.

Now, with the values of η_0 , η_s , and τ_f estimated from the experiments one could determine, at least in principle, the value of the elastic constant κ through Eq. (23) by considering Eqs. (22) and (24), that is,

$$\kappa = \frac{6\eta_0^2}{\pi\eta_s\tau_f} a. \quad (26)$$

The obtained expression shows that the elastic constant display a dependence on the radius a of the probe particle, which is the only arbitrary (free) parameter of the EFM. However, since ζ (or D_0) will also depend on a as in Eq. (14), one can verify that, for both numerical methods (*i.e.*, overdamped dynamics and relaxation simulations), the resulting MSD will be proportional to a^{-1} so that the compliance $J(\tau)$ evaluated via Eq. (4) will not depend on the value of a . Interestingly, such “renormalizability” can be seen as a suitable feature of our methodology since it occurs just as expected from any meaningful microrheological approach. It can be instructive to consider Eqs. (22) and (24) in order to replace a in Eq. (4) so that the compliance can be

rewritten as

$$J(\tau) = \frac{1}{2d D_f \eta_0} \langle \Delta r^2(\tau) \rangle. \quad (27)$$

Even so, Eq. (22) indicates that one still have an implicit dependence of D_f on a , which will be cancelled out by the implicit dependence of the MSD on a as well. In fact, the restriction on the values of the EFM parameters is imposed by experimental data mainly through Eqs. (23) and (24), which only require that the product of the elastic constant and the diffusion coefficient have a specific value, *i.e.*, $\kappa D_0 = k_B T \eta_0^2 / \pi^2 \tau_f \eta_s^2$. For example, in order to obtain the compliance $J(\tau)$ that is displayed in Fig. 3(a), we choose $\kappa D_0 = 12.342$ pN.nm/s, which is consistent with the values of T , η_0 , η_s , and τ_f that were estimated from experiments. The ambiguity in the definitions of D_0 (or D_f), Eq. (22), and κ , Eq. (26), can be eliminated only when one set an arbitrary value to the radius of the probe particles, *e.g.*, $a = 2.8$ μ m as used in Ref.¹¹, which yields $D_0 = 1.69$ nm²/ms and $\kappa = 7.28 \times 10^{-3}$ pN/nm.

In addition, we note that there is some freedom when choosing the physical units of the time increment Δt used in the simulations (see Eqs. (12) and (17)), and usually it is convenient to set it with the same time units that is used to define D_0 . However, it is, in fact, more important that its value is small enough so that it ensures not only numerical stability but also that a free-like diffusion regime with the MSD given by $\langle \Delta r^2(\tau) \rangle \approx 2d D_0 \tau$ is observed. For instance, in order to obtain the numerical data displayed in Fig. 3(a) we consider $\Delta t = 0.1$ ms, which is much shorter than $\tau_0 \approx 33.8$ ms (and it is not displayed in the figure).

Accordingly, as shown in Fig. 3(a), the EFM defined with parameters that were determined from a few limiting values allowed us to show how one can apply the relaxation simulations to obtain the non-markovian dynamics that lead to the whole compliance function $J(\tau)$ that agreed with the experimental curve.

Next, we consider Eq. (7) to obtain the complex shear modulus $G^*(\omega)$ from $J(\tau)$, where the Fourier transform of the compliance $\hat{J}(\omega)$ is evaluated numerically by the method proposed in Ref.⁴² (see Ref.³² for further details). In addition, we evaluate the complex viscosity from $G^*(\omega)$ as

$$\eta^*(\omega) = \frac{G^*(\omega)}{i\omega} . \quad (28)$$

Figures 3(b) and 3(c) indicates that both storage $G'(\omega)$ and loss $G''(\omega)$ modulus, as well as the viscosity $\eta'(\omega) = G''(\omega)/\omega$, present a surprisingly good agreement to the experimental data obtained from PAM chains¹¹. In particular, Fig. 3(b) shows that, at low frequencies, $\omega \ll \tau_f^{-1} \approx 0.3 \text{ rad/s}$, $G'(\omega) \propto \omega^2$ and $G''(\omega) \propto \omega$, which means that the viscosity $\eta'(\omega) = G''(\omega)/\omega$ goes to a constant value, $\eta_0 \approx 460 \text{ mPa.s}$. As shown in Fig. 3(c), $\eta'(\omega)$ tends to a value η_0/N at high frequencies, thus, as mentioned earlier, one can consider those values to estimate the effective number of beads N of the EFM through Eq. (24).

Here, it is important to emphasize that Eqs. (22)-(27), which were obtained for flexible chains, are also valid for an EFM defined with $\kappa_b \neq 0$. Hence, as we discuss below, the same approaches presented in this section can be applied in the study of dilute solutions of semiflexible filaments.

5. RESULTS

In the following we present numerical results obtained for solutions of semiflexible filaments. In particular, we analyse the effect of bending energies on the dynamics of EFMs characterized by both short and long filaments, demonstrating the effectiveness of our relaxation simulations described in Sec. 4.1.

Figure 4 include results obtained for dilute solutions of filaments described by semiflexible EFMs composed by $N = 1000$ beads defined with different values for the bending constant κ_b but with a fixed elastic constant κ . The results presented in Fig. 4 were obtained for long chains with parameters that were arbitrarily chosen in order not only to demonstrate the usefulness of our relaxation simulations, but also to show the effects of bending energies on time scales that are clearly distinguishable on the dynamical quantities, *i.e.*, $\langle \Delta r^2(\tau) \rangle$ and $D(\tau)$, and on the viscoelastic functions, *i.e.*, $G'(\omega)$, $G''(\omega)$, and $\eta'(\omega)$. Importantly, we labelled the results in terms of $A \equiv E'/b$, which is a quantity that is directly related to the bending constant, as $\kappa_b = E/b^4$ and $E' = E/k_B T$ (see Sec. 3.1), and also because the persistent length

L_p of the EFM should be proportional to A . In practice, higher values of κ_b correspond to greater values of A , and the corresponding effective media can be interpreted as EFMs having longer persistent lengths L_p . Nevertheless, one should note that the EFM is used to describe the effective bending energy that result from the coupling between a probe particle and the semiflexible filaments in solution, thus L_p should represent an effective quantity rather than the persistent length of a single semiflexible filament in solution. Here, in order to have numerical values attributed to A (hence to κ_b), we simply choose $k_B T = 4.142 \text{ pN.nm}$ ($T = 300 \text{ K}$), $D_0 = 1 \text{ nm}^2/\text{ms}$, and $b = 1 \text{ nm}$. These choices set values to the elastic constant, $\kappa = 3k_B T/b^2 = 12.426 \text{ pN/nm}$, and to the longest relaxation time, Eq. (23), $\tau_f \approx 3.4 \times 10^4 \text{ ms}$, but not to the viscosity η_0 , so we present just the reduced viscoelastic functions in Figs. 4(c) and 4(d).

Figures 4(a) and 4(b) show that the bending energy lead to significant changes in the dynamics of the beads in the EFM. In particular, the short-time diffusion dynamics observed for the flexible EFM ($A = 0 \text{ nm}$) is altered to an extended subdiffusive regime where $\langle \Delta r^2(\tau) \rangle \propto \tau^\alpha$, with α approaching $3/4$ as the value of A increases. This behaviour is confirmed in Fig. 4(b) by the time-dependent diffusion coefficient $D(\tau)$, from where one can verify that the shortest relaxation time decreases as A (and κ_b) increases, while changes in the bending constant κ_b seems to not alter the longest relaxation time τ_f (at least for $A < 5000 \text{ nm}$). Figure 4(b) indicate that higher values of A lead to a wider range of subdiffusive anomalous behaviour where $D(\tau) \propto \tau^{-1/4}$. By considering a local power-law approximation for the time-dependent diffusion coefficient, *i.e.*, $D(\tau) \propto \tau^\nu$, we computed the numerical derivatives of ν and, from its inflexion points, we determine two characteristic time scales, τ_s and τ_b , which comprise the range of subdiffusive behaviour that is directly related to the introduction of the bending energy, as illustrated for $A = 500 \text{ nm}$ in Fig. 4(b). Interestingly, our results indicate that both characteristic times depend on A in a simple way and, as shown in the inset of Fig. 4(b), $\tau_s \approx 0.3 A^{-1}$ and $\tau_b \approx 0.3 A$. In addition, we observe that, at least for that range of A , the long time diffusion coefficient $D_f = D_0/N$ and the longest relaxation time τ_f remained unaltered, thus they can be conveniently evaluated from Rouse estimates through Eqs. (22) and (23), respectively.

As shown in Figs. 4(c) and 4(d), the changes in the short time dynamics of the beads in the semiflexible EFM clearly modify the high frequency viscoelastic response of the solution. In contrast to the dynamics of the beads in the flexible EFM, which display a characteristic exponent $\alpha = 1/2$ at high frequencies²⁷ (see, *e.g.*, Fig. 2), greater values of A lead to a subdiffusive anomalous behaviour so that the reduced moduli are given by $G'(\omega)/\eta_0 \propto \omega^\alpha$ and $G''(\omega)/\eta_0 \propto \omega^\alpha$, and the relative viscosity is given by $\eta'(\omega)/\eta_0 \propto \omega^{\alpha-1}$, with a characteristic exponent $\alpha \approx 3/4$, in agreement to what have been suggested by previous theoretical and computational studies presented

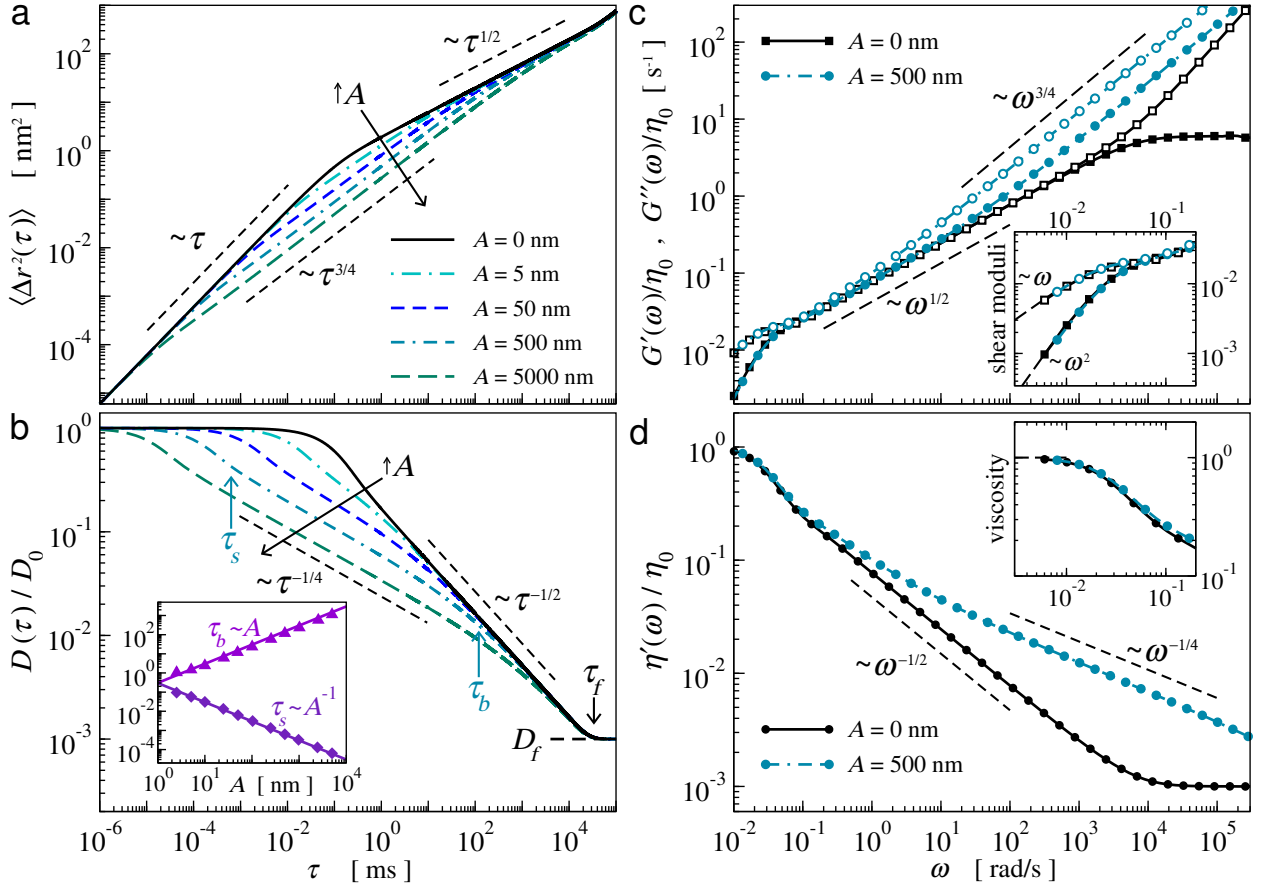


FIG. 4. Effect of bending energies on the dynamics of semiflexible EFMs and the viscoelastic properties of the corresponding solutions. Here we labelled the data in terms of $A = E'/b$, which should be proportional to both the bending constant $\kappa_b = E'k_BT/b^4$ and the persistent length L_p of the EFM. (a) Mean-squared displacement of the m -th bead $\langle \Delta r^2(\tau) \rangle$, Eq. (20); (b) time-dependent diffusion coefficient $D(\tau)$, Eq. (21) (Inset: characteristic times τ_s and τ_b as a function of A); (c) reduced storage modulus $G'(\omega)/\eta_0$ (filled symbols), and loss modulus $G''(\omega)/\eta_0$ (open symbols), obtained from the compliance $J(\tau)$, Eq. (27), through Eq. (7); and (d) reduced viscosity, $\eta'(\omega)/\eta_0$, Eq. (28). Inset panels of (c) and (d) are just zoomed in regions to show the low frequency regimes. In order to clearly demonstrate both the effects of bending and the efficiency of our approach, the relaxation simulations were implemented for EFMs defined with $N = 1000$ and different values of the bending constant κ_b . Results were obtained with a constant external force $F_0 = 1$ pN, $D_0 = 1 \text{ nm}^2/\text{ms}$, $T = 300$ K ($k_BT = 4.142$ pN.nm), $\Delta t = 10^{-6}$ ms, and with a fixed value for the elastic constant $\kappa = 12.426$ pN/nm, so that $\tau_f \approx 3.4 \times 10^4$ ms for all κ_b (or A). Short-dashed (black) lines indicate power-law behaviours observed for the dynamical and rheological quantities.

in the literature^{20,29–31,35,36}. Also, as expected from the dynamics, one can verify from the inset of Figs. 4(c) and 4(d) that the low frequency regimes of the reduced moduli and the reduced viscosity are not altered due to the introduction of the bending energy.

A careful look at Fig. 4(c) indicates that, in addition to the power-law behaviour observed for the shear moduli with a somewhat characteristic exponent $\alpha = 3/4$, the rheology of solutions of semiflexible filaments might display intermediate values of α , also including a transition regime from the flexible behaviour with exponent $\alpha = 1/2$. In order to illustrate that idea we include comparisons between the numerical results obtained from our relaxation simulations and experimental data extracted from microrheology experiments.

For instance, Fig. 5 shows the viscoelastic response

obtained for a dilute solution of DNA³⁴ which is very similar to the behaviour observed for intermediate values of A and long filaments showed in Fig. 4(c), that is, a transition from a subdiffusive regime with $\alpha \approx 1/2$ at intermediate frequencies to a regime where $G'(\omega) \sim G''(\omega) \sim \omega^{3/4}$, at high frequencies. Unfortunately, as shown in the inset of Fig. 5, the frequency-dependent viscosity $\eta'(\omega)$ obtained from the experiments do not include data at sufficiently high frequencies which would have allowed us to determine the exact number of beads N of the EFM via Eq. (24). Even so, by arbitrarily choosing $N = 1000$ as well as by considering $\kappa D_0 = 31.846$ pN.nm/ μs in order to match the experimentally estimated viscosity, $\eta_0 \approx 30$ mPa.s, temperature, $T = 23^\circ\text{C}$, and longest relaxation time, $\tau_f \approx 0.013$ s, we were able to attain a quantitative agreement between the

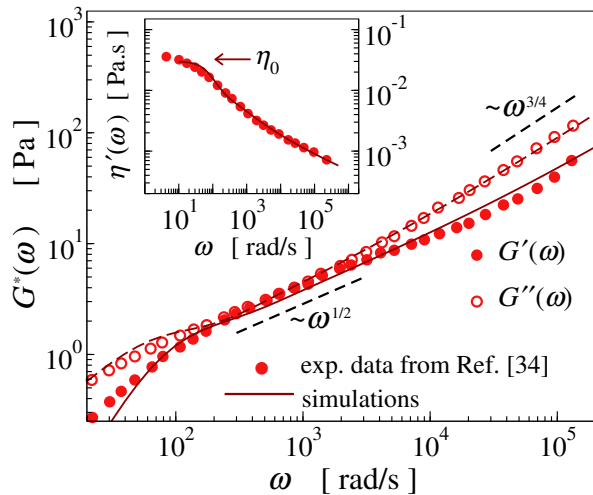


FIG. 5. Comparison between the shear moduli, $G'(\omega)$ and $G''(\omega)$, obtained from relaxation simulations (continuous lines), as described in Sec. 4.2, and the experimental data (circles) obtained for a 1 mg/mL 5.8 kilobase DNA solution³⁴. The inset panel displays the frequency-dependent viscosity evaluated from the loss modulus, $\eta'(\omega) = G''(\omega)/\omega$. Relaxation simulations were performed with $F_0 = 1$ pN, $N = 1000$, $D_0 = 14.45$ nm²/μs, $\kappa = 2.2$ pN/nm ($b \approx 2.36$ nm), $\kappa_b = 367.28$ pN/nm ($A \approx 1179$ nm), and $\Delta t = 10^{-6}$ μs, in order to be consistent with the given experimental conditions, *i.e.*, $\eta_0 \approx 30$ mPa.s, $T \approx 23^\circ\text{C}$ ($k_B T = 4.086$ pN.nm), and $\tau_f \approx 0.013$ s. The values of D_0 and κ were determined respectively through Eqs. (22) and (26) by setting $a = 0.5$ μm, which is the radius of the probe particles specified in Ref.³⁴. By considering Eq. (25), the estimated number density of DNA molecules in solution is equal to $n_f \approx 42 \times 10^{13}$ cm⁻³, which yields a molecular weight of 1.42×10^6 g/mol, in a reasonable agreement with the size and the concentration of DNA used in the experiments.

numerical results and the experimental data. Here, it is worth noting that the viscosity $\eta'(\omega)$ displayed in the inset of Fig. 5 spans several orders of magnitude, so that, according to Eq. (24), only large values of N would be suitable to describe the experimental data.

Next, we include in Fig. 6 a comparison between the numerical results obtained from our relaxation simulations and the experimental data on solutions of collagen at 2 mg/mL extracted from Ref.⁴³. Unfortunately, the experimental data of Ref.⁴³ do not include the low frequency regime of the viscoelastic functions, even so we use the frequency-dependent viscosity $\eta'(\omega)$ to estimate the number of beads of the EFM as $N = 15$, which gives $\eta_0 = N\eta_s \approx 22.4$ mPa.s, and we also consider $\tau_f \approx 1.023$ s, so that Eq. (23) yields $\kappa D_0 \approx 90.45$ pN.nm/s. Although the effective number of beads is small as in the case of PAM, it is worth mentioning that, as in the case of DNA, several relaxation simulations were required to determine a suitable value for the bending constant κ_b in order to obtain meaningful viscoelastic response functions over the full range of frequencies. The results presented in Fig. 6 indicate that the exponent α

observed for the power-law behaviour of the shear moduli present a value between 1/2 and 3/4 at an intermediate frequency range. The value of $\alpha \approx 0.7$ is corroborated by the behaviour of the frequency-dependent viscosity $\eta'(\omega) \propto \omega^{\alpha-1}$ which is displayed in the inset panel. As suggested in Ref.⁴³, such intermediate behaviour between flexible and semiflexible could be explained due to ratio between the short contour length ($L \approx 300$ nm) and the persistent length ($L_p \approx 15 - 160$ nm) of the collagen molecules, which would put the viscoelastic response of the corresponding solution in a crossover region. However, the number density of filaments in solution estimated through Eq. (25) is $n_f \approx 0.03 \times 10^{13}$ cm⁻³, which is a very low value for the nominal concentration of 2 mg/mL. This value of n_f leads to a “molecular” weight of 2.2×10^9 g/mol, indicating that the filamentous structures in solution might be, in fact, self-assembled fibers that are much larger than the 300 kDa collagen molecules assumed in Ref.⁴³. Interestingly, the presence of large supramolecular structures composed by thousands of macromolecules might explain why the EFM required only a rather small effective number of beads in order to describe the viscoelasticity of dilute solutions of semiflexible collagen molecules.

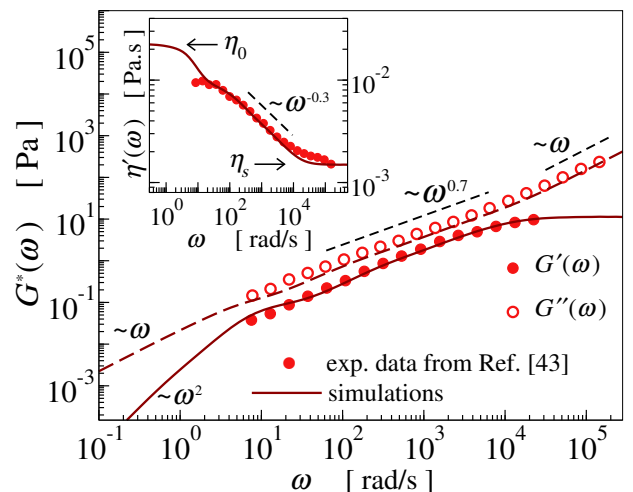


FIG. 6. Comparison between the viscoelastic properties obtained from relaxation simulations (lines), as described in Sec. 4.2, and the experimental data (circles) extracted from Ref.⁴³, which corresponds to solutions of collagen macromolecules at 2 mg/mL. The main panel shows the storage modulus (filled circles), $G'(\omega)$, and the loss modulus (open circles), $G''(\omega)$, while the viscosity $\eta'(\omega) = G''(\omega)/\omega$ is displayed in the inset panel. Relaxation simulations were performed with $F_0 = 1$ pN, $N = 15$, $D_0 = 68.67$ nm²/ms, $\kappa = 1.317 \times 10^{-3}$ pN/nm ($b \approx 96$ nm), $\kappa_b = 74.1 \times 10^{-3}$ pN/nm ($A \approx 1.62 \times 10^4$ nm), and $\Delta t = 10^{-6}$ ms, in order to be consistent with the given experimental conditions, *i.e.*, $T \approx 21^\circ\text{C}$ ($k_B T = 4.059$ pN.nm), $\eta_s \approx 1.49$ mPa.s, $\eta_0 = N\eta_s \approx 22.4$ mPa.s, and $\tau_f \approx 1.023$ s. The specific values of κ and D_0 were determined by setting the radius of the probe particles equal to $a = 2.1$ μm as in Ref.⁴³.

It is worth noting that, in general, the effective number of beads N of the EFM is constrained by the experimentally available information through Eq. (24), but one can choose any arbitrary value for the radius a of the probe particles (see Sec. 4.2). Although the viscoelastic functions $J(\tau)$, $G'(\omega)$, and $G''(\omega)$ obtained from our approach do not depend on the value of a , it is advisable to restrict it to the micron-sized range as in the most of microrheological experiments¹ in order to avoid unphysical values for the effective coupling constants κ , Eq. (26), and κ_b . In addition, we emphasize that the application of the EFM and the FDT should be limited to cases where microrheological approaches are valid, in particular, when the so-called Stokes and Einstein components are valid (see Ref.²³).

6. CONCLUDING REMARKS

In this work we present efficient relaxation simulations as an alternative numerical method that allow one to evaluate the viscoelastic response of both flexible and semiflexible filament solutions. In particular, our study indicates that the evaluation of the MSD and the time-dependent diffusion coefficient of the probe particles described by the EFM is orders of magnitude quicker for the relaxation simulations in comparison to the stochastic approach. In addition, by considering a modelling approach that is based on microrheology, we have established useful relations that allowed us to obtain the shear moduli and the viscosity of unentangled filament solutions without having to resort to shearing protocols that are used for solutions with cross-linked and tightly entangled filaments.

Despite of the fact that we have used a simple modelling approach, the quantitative agreement between our numerical results and the experimental data presented in Figs. 5 and 6 demonstrate the effectiveness of the EFM in obtaining meaningful frequency-dependent viscoelastic response functions for dilute solutions of semiflexible filaments. We believe that it could encourage the use of the relaxation methodology combined with more detailed approaches. In particular, it might be interesting to extend the EFM to incorporate excluded volume effects in order to describe other physical scenarios, *e.g.*, semi-dilute solutions^{33,44}. Also, since the relaxation simulations have been previously adapted to obtain the dynamics of random flexible polymers networks through an averaging procedure¹⁵, one might also extend it to more complex solutions which display locally distributed viscoelastic properties^{39,45,46}. Even so, one must realize that although the approach described in Sec. 4.2 is useful to provide estimates for the parameters N , κ , and D_0 , the EFM is not a microscopic, *i.e.*, molecular-based, model, hence it lacks the predictive power that one may desire in many real-life applications. For solutions of semiflexible polymers, in particular, there might be still the need to perform a considerable large number of simulations

in order to test EFMs defined with different values of the bending constant κ_b until one obtain appropriate viscoelastic functions, *i.e.*, $G'(\omega)$, $G''(\omega)$, and $\eta'(\omega)$, in a wide range of frequencies. Nevertheless, this also emphasizes the importance of the efficiency of our relaxation approach presented in Sec. 4.1 when compared to the stochastic simulations described in Sec. 3.2.

Finally, it is worth mentioning that, since the theoretical basis of the relaxation simulations is the fluctuation-dissipation theorem, the determination of the mean-squared displacement and the time-dependent diffusion coefficient of the beads through Eqs. (20) and (21), respectively, does not need to be based neither on stochastic simulations or on the EFM to be accomplished. Hence, one might try to explore those equations together with Eqs. (4) and (7), just as it has been done in microrheology experiments¹¹, and associate them with molecular-based simulations in order to provide the dynamics of a probe particle which takes into account its interactions with all solvent and polymeric molecules in solution. Alternatively, one may consider systematic coarsening procedures based also on more fundamental (*i.e.*, molecular-based) simulations¹⁶ which could be used, for instance, to develop improved EFMs by establishing effective potentials for which the dynamics of the probe particle is affected by specific microscopic conditions of the polymers in solution.

L. G. Rizzi acknowledges the financial support of the Brazilian agencies CNPq (Grants N° 306302/2018-7 and N° 426570/2018-9) and FAPEMIG (Process APQ-02783-18), and L. K. R. Duarte thanks the scholarship from the Brazilian agency CAPES.

REFERENCES

- ¹L. G. Rizzi and M. Tassieri, "Microrheology of biological specimens," in: *Encyclopedia of Analytical Chemistry* (2018).
- ²R. H. Pritchard, Y. Y. S. Huang, and E. M. Terentjev, "Mechanics of biological networks: from the cell cytoskeleton to connective tissue," *Soft Matter*, **10**, 1864 (2014).
- ³C. Lang, J. Hendricks, Z. Zhang, N. K. Reddy, J. P. Rothstein, M. P. Lettinga, J. Vermant, and C. Clasen, "Effects of particle stiffness on the extensional rheology of model rod-like nanoparticle suspensions," *Soft Matter*, **15**, 833 (2019).
- ⁴C. Broedersz and F. MacKintosh, "Modeling semiflexible polymer networks," *Rev. Mod. Phys.* **86**, 995 (2014).
- ⁵L. G. Rizzi, D. A. Head, and S. Auer, "Universality in the morphology and mechanics of coarsening amyloid fibril networks," *Phys. Rev. Lett.* **114**, 078102 (2015).
- ⁶L. G. Rizzi, S. Auer, and D. A. Head, "Importance of non-affine viscoelastic response in disordered fibre networks," *Soft Matter*, **12**, 4332 (2016).
- ⁷F. Meng and E. M. Terentjev, "Theory of semiflexible filaments and networks," *Polymers* **9**, 52 (2017).
- ⁸C. Cruz, F. Chinesta, and G. Régner, "Review on the brownian dynamics simulation of bead-rod-spring models encountered in computational rheology," *Arch. Comput. Methods Eng.* **19**, 227 (2012).
- ⁹R. G. Larson, "The rheology of dilute solutions of flexible polymers: Progress and problems," *J. Rheol.* **49**, 1 (2005).
- ¹⁰F. Gittes, B. Schnurr, P. D. Olmsted, F. C. MacKintosh, and C. F. Schmidt, "Microscopic viscoelasticity: Shear moduli of soft materials determined from thermal fluctuations," *Phys. Rev. Lett.* **79**, 3286 (1997).

- ¹¹M. Tassieri, T. A. Waigh, J. Trinick, A. Aggeli, and R. M. L. Evans, "Analysis of the linear viscoelasticity of polyelectrolytes by magnetic microrheometry - Pulsed creep experiments and the one particle response," *J. Rheol.* **54**, 117 (2010).
- ¹²D. A. Head, E. Ikebe, A. Nakamasu, P. Zhang, L. G. Villaruz, S. Kinoshita, S. Ando, and D. Mizuno, "High-frequency affine mechanics and nonaffine relaxation in a model cytoskeleton," *Phys. Rev. E* **89**, 042711 (2014).
- ¹³P. Licinio and A. V. Teixeira, "Anomalous diffusion of ideal polymer networks," *Phys. Rev. E* **56**, 631 (1997).
- ¹⁴P. Licinio and A. V. Teixeira, "Relaxation of ideal polymer networks," *Philos. Mag. B* **78**, 171 (1998).
- ¹⁵A. V. Teixeira and P. Licinio, "Dynamics of swollen fractal networks," *Europhys. Lett.* **45**, 162 (1999).
- ¹⁶T. E. Gartner III and A. Jayaraman, "Modeling and simulations of polymers: A roadmap," *Macromolecules* **52**, 755 (2019).
- ¹⁷T. A. Waigh, "Advances in the microrheology of complex fluids," *Rep. Prog. Phys.* **79**, 074601 (2016).
- ¹⁸R. G. Larson, *The Structure and Rheology of Complex Fluids* (Oxford University Press, 1999).
- ¹⁹J. D. Ferry, *Viscoelastic properties of polymers*, 3rd ed. (John Wiley & Sons, 1980).
- ²⁰M. Rubinstein and R. H. Colby, *Polymer Physics* (Oxford University Press, 2003).
- ²¹M. Doi, *Soft Matter Physics* (Oxford University Press, 2013).
- ²²S.-P. Li, G. Zhao, and H.-Y. Chen, "The relationship between steady shear viscosity and complex viscosity," *J. Disper. Sci. Technol.* **26**, 415 (2005).
- ²³T. M. Squires and T. G. Mason, "Fluid mechanics of microrheology," *Annu. Rev. Fluid Mech.* **42**, 413 (2010).
- ²⁴M. Tassieri, F. D. Giudice, E. Robertson, N. Jain, B. Fries, R. Wilson, A. Glidle, F. Greco, P. A. Netti, P. L. Maffettone, T. Bicanic, and J. M. Cooper, "Microrheology with optical tweezers: Measuring the relative viscosity of solutions 'at a glance'," *Sci. Rep.* **5**, 8831 (2015).
- ²⁵J. Xu, V. Viasnoff, and D. Wirtz, "Compliance of actin filament networks measured by particle-tracking microrheology and diffusing wave spectroscopy," *Rheol. Acta* **37**, 387 (1998).
- ²⁶T. G. Mason, "Estimating the viscoelastic moduli of complex fluids using the generalized stokes-einstein equation," *Rheol. Acta* **39**, 371 (2000).
- ²⁷M. Doi and S. F. Edwards, *The Theory of Polymer Dynamics* (Oxford University Press, 1986).
- ²⁸W. Paul, K. Binder, D. W. Heermann, and K. Kremer, "Dynamics of polymer solutions and melts. Reptation predictions and scaling of relaxation times," *J. Chem. Phys.* **95**, 7726 (1991).
- ²⁹M. Pasquali, V. Shankar, and D. C. Morse, "Viscoelasticity of dilute solutions of semiflexible polymers," *Phys. Rev. E* **64**, 020802 (2001).
- ³⁰A. Nikoubashman, A. Milchev, and K. Binder, "Dynamics of single semiflexible polymers in dilute solution," *J. Chem. Phys.* **145**, 234903 (2016).
- ³¹V. Shankar, M. Pasquali, and D. C. Morse, "Theory of linear viscoelasticity of semiflexible rods in dilute solution," *J. Rheol.* **46**, 1111 (2002).
- ³²M. Tassieri, R. M. L. Evans, R. L. Warren, N. J. Bailey, and J. M. Cooper, "Microrheology with optical tweezers: Data analysis," *New J. Phys.* **14**, 115032 (2012).
- ³³E. Sarmiento-Gomez, D. Montalvan-Sorrosa, C. Garza, J. Mas-Oliva, and R. Castillo, "Rheology and DWS microrheology of concentrated suspensions of the semiflexible filamentous fd virus," *Eur. Phys. J. E* **35**, 35 (2012).
- ³⁴B. A. Krajina, C. Tropini, A. Zhu, P. DiGiacomo, J. L. Sonnenburg, S. C. Heilshorn, and A. J. Spakowitz, "Dynamic light scattering microrheology reveals multiscale viscoelasticity of polymer gels and precious biological materials," *ACS Cent. Sci.* **3**, 1294 (2017).
- ³⁵P. Dimitrakopoulos, J. F. Brady, and Z.-G. Wang, "Short- and intermediate-time behavior of the linear stress relaxation in semiflexible polymers," *Phys. Rev. E* **64**, 050803 (2001).
- ³⁶E. F. Koslover and A. J. Spakowitz, "Multiscale dynamics of semiflexible polymers from a universal coarse-graining procedure," *Phys. Rev. E* **90**, 013304 (2014).
- ³⁷D. Panja, "Generalized Langevin equation formulation for anomalous polymer dynamics," *J. Stat. Mech.* **2010**, L02001 (2010).
- ³⁸D. Panja, "Anomalous polymer dynamics is non-markovian: Memory effects and the generalized Langevin equation formulation," *J. Stat. Mech.* **2010**, P06011 (2010).
- ³⁹L. G. Rizzi, "Microrheological approach for the viscoelastic response of gels," *J. Rheol.* **64**, 969 (2020).
- ⁴⁰A. E. Likhtman, S. K. Sukumaran, and J. Ramirez, "Linear viscoelasticity from molecular dynamics simulation of entangled polymers," *Macromolecules* **40**, 6748 (2007).
- ⁴¹D. T. Gillespie, "Fluctuation and dissipation in Brownian motion," *Am. J. Phys.* **61**, 1077 (1993).
- ⁴²R. M. L. Evans, M. Tassieri, D. Auhl, and T. A. Waigh, "Direct conversion of rheological compliance measurements into storage and loss moduli," *Phys. Rev. E* **80**, 012501 (2009).
- ⁴³M. Shayegan and N. R. Forde, "Microrheological characterization of collagen systems: From molecular solutions to fibrillar gels," *Plos ONE* **8**, e70590 (2013).
- ⁴⁴X. Chen, Y. Zhang, H. Wang, S.-W. Wang, S. Liang, and R. H. Colby, "Solution rheology of cellulose in 1-butyl-3-methyl imidazolium chloride," *J. Rheol.* **55**, 485 (2011).
- ⁴⁵N. Nahali and A. Rosa, "Nanoprobe diffusion in entangled polymer solutions: Linear vs. unconcatenated ring chains," *J. Chem. Phys.* **148**, 194902 (2018).
- ⁴⁶T. N. Azevedo and L. G. Rizzi, "Microrheology of filament networks from Brownian dynamics simulations," *J. Phys.: Conf. Ser.* **1483**, 012001 (2020).